Atmospheric Environment 187 (2018) 84–92

Contents lists available at ScienceDirect

Atmospheric Environment

journal homepage: www.elsevier.com/locate/atmosenv

Investigation of ambient aerosol effective density with and without using a catalytic stripper

Yue Lin[a,b], Roya Bahreini[c], Stephen Zimmerman[c], Emmanuel A. Fofie[f], Akua Asa-Awuku[f], Kihong Park[d], Seung-Bok Lee[e], Gwi-Nam Bae[e], Heejung S. Jung[a,b,*]

[a] Department of Mechanical Engineering, University of California Riverside, Riverside, CA, USA
[b] College of Engineering-Center for Environmental Research and Technology (CE–CERT), University of California Riverside, Riverside, CA, USA
[c] Department of Environmental Sciences, University of California Riverside, Riverside, CA, USA
[d] School of Earth Sciences and Environmental Engineering, Gwangju Institute of Science and Technology, Gwangju, South Korea
[e] Center for Environment, Health and Welfare Research, Korea Institute of Science and Technology, Seoul, South Korea
[f] Chemical and Biomolecular Engineering, University of Maryland, College Park, MD, USA

ARTICLE INFO

Keywords:
Riverside
Secondary organic aerosol
Effective density
Catalytic stripper
Thermal denuder
Receptor

ABSTRACT

Size-resolved effective densities of ambient aerosols in Riverside, CA were determined over 4 periods during 2015–2016. A DMA-CPMA-CPC technique was used to measure effective density for particles with selected diameters of 50, 70, 101 and 152 nm. A catalytic stripper (CS) was used alternately to remove the volatile fraction of aerosol before density measurements. Aerosol non-refractory composition measurement was conducted in June 2016 campaign to understand the effect of chemical composition on particle density. The average densities for particles over all the measurement campaigns over BP mode (i.e. bypassing the CS) were 1.17 g/cm^3 at 50 nm and 1.25–1.28 g/cm^3 at 70, 101 and 152 nm. The average density after CS conditioning (CS mode) showed a decreasing trend from 1.22 g/cm^3 to 1.04 g/cm^3, with increase in the selected size, and a mass fractal dimension (D_f) of 2.85. Both the BP and CS mode particles showed the lowest effective density at 6–9 am and highest density at 11 a.m.-3 pm. The diurnal variation of density for both modes became more intensive as particle size increased. The variation was also more intense for the CS mode compared to the BP mode. Organic aerosol and ammonium nitrate mass in the size range of density measurements correlated well positively (R^2 = 0.78) and negatively (R^2 = 0.62), respectively with BP mode effective density. The study provides an update to the aerosol density profiles of a well-known receptor site (Riverside, CA) and investigates the transformation of particles in different seasons. The effective density profiles will be used in a follow-up study to better estimate the respiratory-deposited ambient aerosol mass.

1. Introduction

Atmospheric aerosol plays an important role in human health, air quality, and climate change. Atmospheric aerosol is complex and dynamic in its chemical composition and physical mixing state. Effective density is an important property to understand the mixing state, transport, and depositional characteristics of particles in the ambient atmosphere and human respiratory system. Conventionally, average bulk density is used to convert lung-deposited particle number to mass assuming spherical particle shape, which leads to some degree of uncertainty in the estimate of the deposited mass.

Since McMurry et al. (2002) have developed an online size-resolved effective density measurement method using Differential Mobility Analyzer (DMA)-Aerosol Particle Mass analyzer (APM) technique, this technique has been applied to fresh soot and ambient aerosol to examine morphology and mass-mobility relationships (Geller et al., 2006; Levy et al., 2014; Rissler et al., 2014).

Effective density, ρ_{eff}, is defined as the ratio of particle mass (m) to volume of a sphere with the mobility equivalent diameter (d_m):

$$\rho_{eff} = \frac{6m}{\pi d_m^3} \quad (1)$$

The mass-mobility exponent (D_m) is an indirect measure of the morphology of irregularly shaped fractal-like particles. D_m can be determined from known effective densities of particles at different mobility sizes (Park et al., 2003):

$$\rho_{eff} = C d_m^{D_m - 3} \quad (2)$$

* Corresponding author. Department of Mechanical Engineering, University of California Riverside, 900 University Ave, Riverside, CA 92521, USA.
E-mail address: heejung@engr.ucr.edu (H.S. Jung).

https://doi.org/10.1016/j.atmosenv.2018.05.063
Received 17 January 2018; Received in revised form 26 May 2018; Accepted 28 May 2018
Available online 29 May 2018
1352-2310/

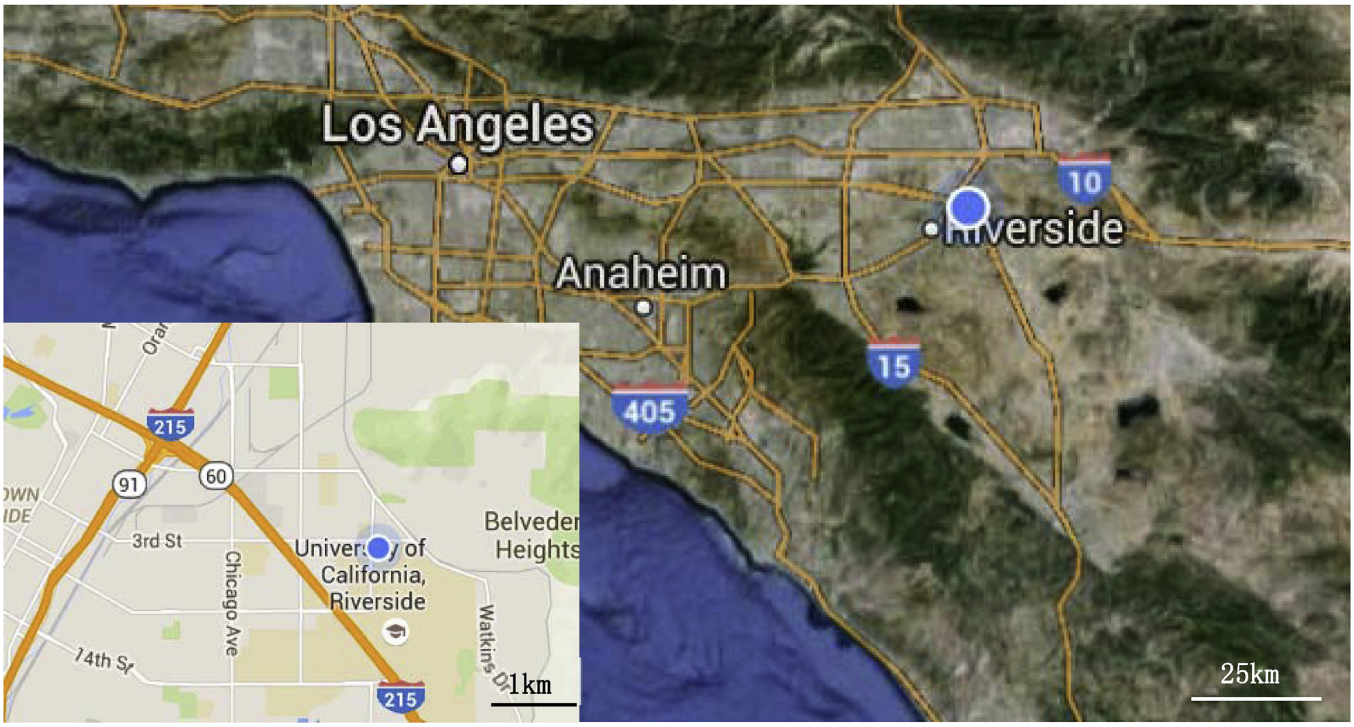

Fig. 1. Map of the sampling site and its distance from the closest highway.

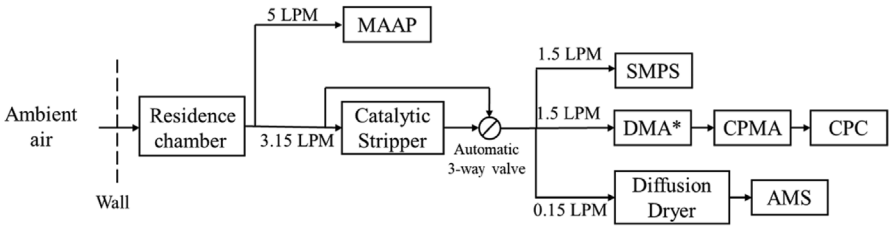

Fig. 2. Schematic of the experimental setup.

The mass-mobility exponent is the same as the fractal dimension, D_f, when the ratio between radius of gyration (R_g) and mobility diameter (d_m) is constant (Maricq and Xu, 2004; Park et al., 2003; Sorensen, 2011).

ρ_{eff} and D_f (or D_m) can be determined by measuring particle mass at different mobility diameters using a DMA- APM system (McMurry et al., 2002) or DMA-centrifugal particle mass analyzer (CPMA) (Olfert and Collings, 2005). The CPMA technique works similarly to APM and has a better instrument inversion transfer function than the APM (Olfert et al., 2007).

The number of studies on particle effective density of ambient aerosols has gradually increased thanks to the establishment of measurement methods and advancement of instrumentation. McMurry et al. (2002) demonstrated capability of DMA-APM system and applied it first for the measurement of effective density of ambient aerosol in Atlanta, GA. They showed the measured density of 1.5–1.7 g/cm^3 agrees with the density calculated based on chemical composition for two selected sizes of 107 and 309 nm particles. Using the same technique, Geller et al. (2006) conducted measurement at various locations in Los Angeles Basin. They observed bimodal density distributions at a location where both traffic and background aerosols were present. They also showed that effective density is driven by photochemistry and meteorology at a receptor site in Riverside, California. The particle effective density of 50 nm particles rapidly dropped from 1.4 g/cm^3 in the mid afternoon to a value of 1.2 g/cm^3 by sunset. The value of 1.2 g/cm^3 is an assumed density for organic aerosol by Turpin and Lim (2001). Spencer et al. (2007) confirmed that effective density varies dynamically, as much as 40%, within 16 h in Riverside, CA during photochemical seasons. They found a correlation between effective density and ambient water content. However, they assumed the correlation might be an artifact due to evaporation in the aerodynamic lens of their aerosol mass spectrometer. Levy et al. (2014) conducted continuous density measurements at US-Mexico border near Tijuana, Mexico for one-week in June, 2010. They reported mixing state and effective density of ambient particles in the size range of 46–240 nm. They showed that the 46 nm particles have the most distinctive diurnal cycle, with the lowest density in the afternoon (at 1–4 pm) likely associated with fresh black carbon emission from vehicles, and the highest in the early morning (at 1–4 a.m.), suggesting the presence of primary organic aerosol. Levy et al. (2013) also conducted density measurement in Houston, Texas. They showed that the effective density has a minimum during morning rush hour and it increases from morning to the afternoon (i.e. 7 a.m. to 5 p.m.) likely due to particle-phase sulfate and oxidized organic components. Rissler et al. (2014) conducted semi-continuous density measurement at an open street canyon in central Copenhagen, Denmark during winter season. They reported both soot and more dense particles were present in 50–400 nm size range. Additionally, they used a thermal denuder in-between DMA and APM and measured the volatile mass fraction of soot as ~10% and those of dense particles as ~80–100%. Yin et al. (2015) conducted a five-week long

Table 1
Summary of the meteorological condition.

Measurement period	9/16/2015–9/23/2015	10/22/2015–10/30/2015	3/1/2016–3/13/2016	6/6/2016–6/13/2016
Ambient temperature (°C)	20–42	16–33	5–27	15–31
Relative humidity (%)	13–85	9–85	17–93	32–90
(average ± standard deviation)	(55.4 ± 19.9)	(41.5 ± 21.5)	(62.8 ± 18.6)	(64.9 ± 15.4)

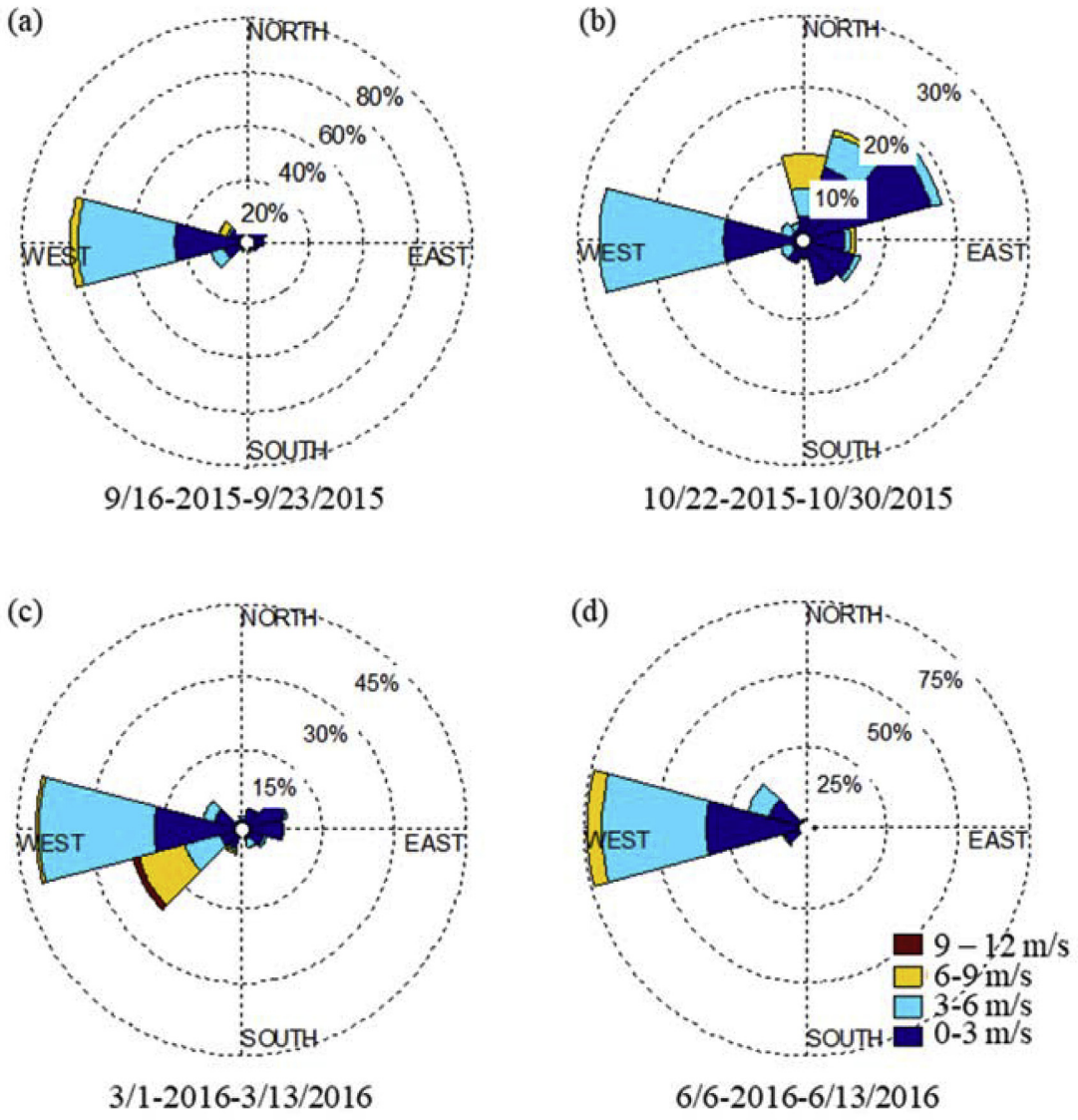

Fig. 3. Wind rose in during the four measurement periods.

measurement in Shanghai, China during December, 2012–January, 2013. They found effective density increased with increasing particle size. They also reported a high correlation between effective density and mass fraction of secondary inorganic aerosol.

The previous studies have reported particle effective density in various locations and specific seasons. In the current study, we collected density data in different seasons throughout a year, along with size-dependent, non-refractory aerosol composition measured by a compact time-of-flight aerosol mass spectrometer (mini-C-ToF-AMS or mAMS, Aerodyne Research Inc.). The (CS)-DMA-CPMA system measured effective density of ambient particles in Riverside, CA in the size range of 50–152 nm, where the alveolar and tracheobronchial deposition efficiency is high (Oberdörster et al., 2005). While Rissler et al. (2014) measured the volatile mass fraction, our approach measures effective density of the non-volatile core particles. Fractal dimensions determined from the current study will reveal the degree of restructuring of the core particles. Riverside, located in Los Angeles (LA) basin, is a well-known receptor site of traffic emissions from LA. Vehicular exhaust particles are transported eastward from LA while undergoing photochemical processes, and occasionally trapped in Riverside by surrounding mountains and stagnant air at this site, (Fig. 1). We conducted continuous measurement of effective density with the overall aim of constraining the inhalable mass budget of ambient aerosol. Diurnal evolution of effective density has significant implications on composition and mass of PM deposited onto the lung. The objective of the current study is to understand the evolution of effective density of particles in Riverside, CA at different seasons of the year. A follow-up study will use the findings of this study and estimate the mass budget of

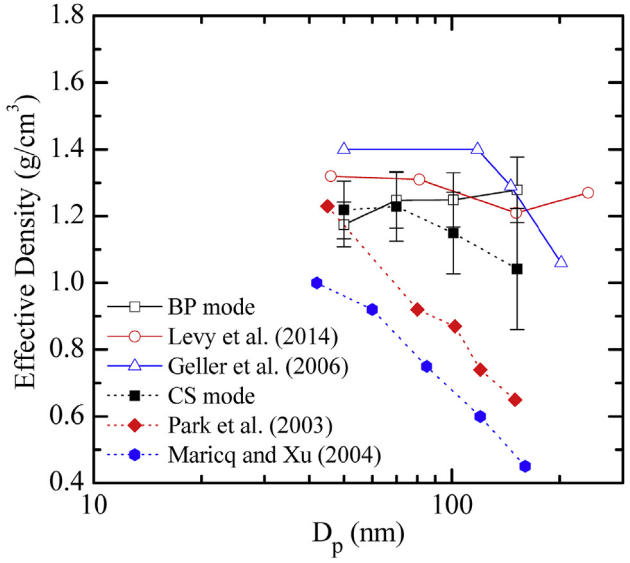

Fig. 4. Average effective densities over all the measurement periods for BP and CS modes. Data from previous studies are also included for comparison.

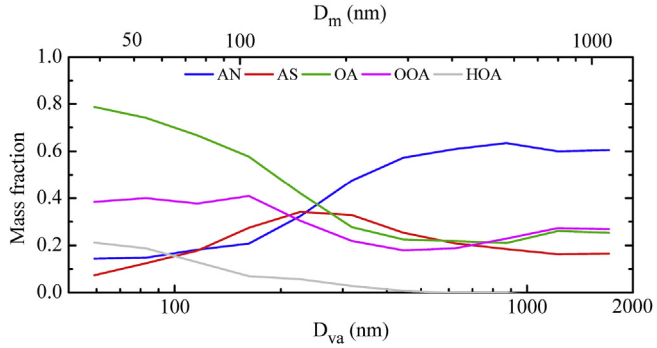

Fig. 5. Mass fraction of dominant non-refractory species measured by mAMS during June 2016.

aerosol that could potentially deposit in human lungs.

2. Experimental

2.1. Measurement location and period

The measurements were conducted on the second floor of the Geology building at the University of California, Riverside (33.974762, −117.326313). The sampling location is 0.55 km away from the nearest highway, State Route 60, and 3.6 km away from highway 91 (Fig. 1). The measurements were performed in four periods during summer, fall, and spring seasons: 9/16/2015–9/23/2015, 10/22/2015–10/30/2015, 3/1/2016–3/13/2016, 6/6/2016–6/15/2016, continuously (24 h per day) in each measurement duration.

2.2. Instrumentation

The general experimental setup is shown in Fig. 2. Each density measurement required 7–9 min. Ambient particles were sampled through a 50 L residence chamber, to provide a pseudo-steady state condition for each measurement. All instruments were located inside the building next to the sampling window. The sampling probe protruded out of the window with the exposed length of 1.5 m upstream of the chamber. A lab-made Catalytic Stripper (Abdul-Khalek and Kittelson, 1995; Martin, 2003) operating at 300 °C was employed to remove volatile particle fraction. A three-way solenoid valve (ASCO Valve, Inc, Novi, MI.) was programmed to switch the flow passage between bypass (BP mode) and Catalytic Stripper (CS mode) every 10 min. A DMA-CPMA-CPC (DMA model 3081, TSI, Inc.; CPMA, Cambustion, Limited; CPC model 3022, TSI, Inc.) system was placed downstream of the solenoid valve to measure particle effective density, once every 10 min. Four mobility diameters (d_m = 50, 70, 101,152 nm) were selected. Effective density and fractal dimension values were calculated using Equations (1) and (2), given the mass corresponding to the mode in the scan data and the d_m selected by DMA. More detailed description on applying CPMA for density measurements can be found in Olfert and Collings (2005).

A Multi-angle Absorption Photometer (MAAP Thermo Scientific model 5012) was deployed in June 2016 to measure the black carbon mass (Petzold et al., 2002). mAMS was deployed in June 2016 to characterize the non-refractory chemical nature of particles, downstream of a silica gel diffusion drier. Composition-dependent collection efficiency correction was applied to the bulk mAMS concentrations (Middlebrook et al., 2012). In order to compare the mAMS mass distribution data that are provided in vacuum aerodynamic diameter (d_{va}) with density data in the electrical mobility diameter, the following relationship was used:

$$d_{va} = d_m \frac{\rho_m}{\rho_0} S \quad (3)$$

Where S is the Jayne shape factor, usually assumed to be 1 for spherical and < 1 for non-spherical particles, ρ_m is material density, and ρ_0 is standard density (1 g/cm^3) (DeCarlo et al., 2004). Here with lack of the Jayne shape factor, we roughly estimate the d_{va} by using an averaged material density of ρ_m = 1.53 g/cm^3, using 10-min average non-refractory and BC composition and assuming density of 1.75 g/cm^3 for ammonium nitrate and ammonium sulfate, 1.3 g/cm^3 for organic aerosol (OA), and 1.8 g/cm^3 for BC (Cross et al., 2007; Middlebrook et al., 2012; Park et al., 2003). In addition with assuming S = 1, d_m = 50–152 nm corresponds to d_{va} = 77–233 nm. See Supplemental Information for further details.

Early studies (McMurry et al., 2002; Olfert et al., 2007) have used poly styrene latex spheres (PSLs) to calibrate DMA-APM and DMA-CPMA systems for density measurement. In cases where the mode diameter is selected from a dried stream of nebulized PSL particles, it is known that there is up to 7% error in detecting 100 nm standard reference material (SRM) 1963 using well-calibrated DMA systems (Mulholland et al., 1999). A well calibrated DMA size selection is known to be within ± 3% (Kinney et al., 1991) in the size range of our interest, which is comparable to the accuracy of commercially available PSLs. Voltages for DMA were confirmed to be accurate within 1%, the sheath flow was within 1.5%, and sample and monodisperse flow were within 5% of the set values. Calibration tests were conducted using PSLs (Nanospheres, Thermofisher) at the four selected mobility diameters (46 ± 2 nm, 70 ± 3 nm, 102 ± 3 nm, 147 ± 3 nm) which correspond to the nominal average diameters of the PSL. Errors in determined density values ranged from −6 to 5% compared to the literature values. Additional calibration tests were conducted for the four selected sizes using NaCl. As NaCl aerosol is not spherical, a shape factor of 1.08 was taken into account by solving the implicit equation for slip correction factor. The uncertainty in the determined density from NaCl calibration tests ranged from 4 to 7%. We chose not to use the voltage method Park et al. (2003) and Olfert et al. (2007) proposed to calibrate DMA-CPMA because newer models of CPMA are more reliable with full commercialization of the instrument, with the uncertainty being at ~ 4% for 95% confidence interval (see section 3 of Symonds et al. (2013)). Errors with the voltage calibration method can be as large as that of PSLs. Additionally, we chose to change both the rotational speed (rpm) and voltage of the CPMA to have the same mass resolution for all measurements. The size based mass resolution parameter R_s is defined as the mass setpoint divided by the full width half maximum of the instrument's transfer function in the size domains. We set R_s as 3 for all

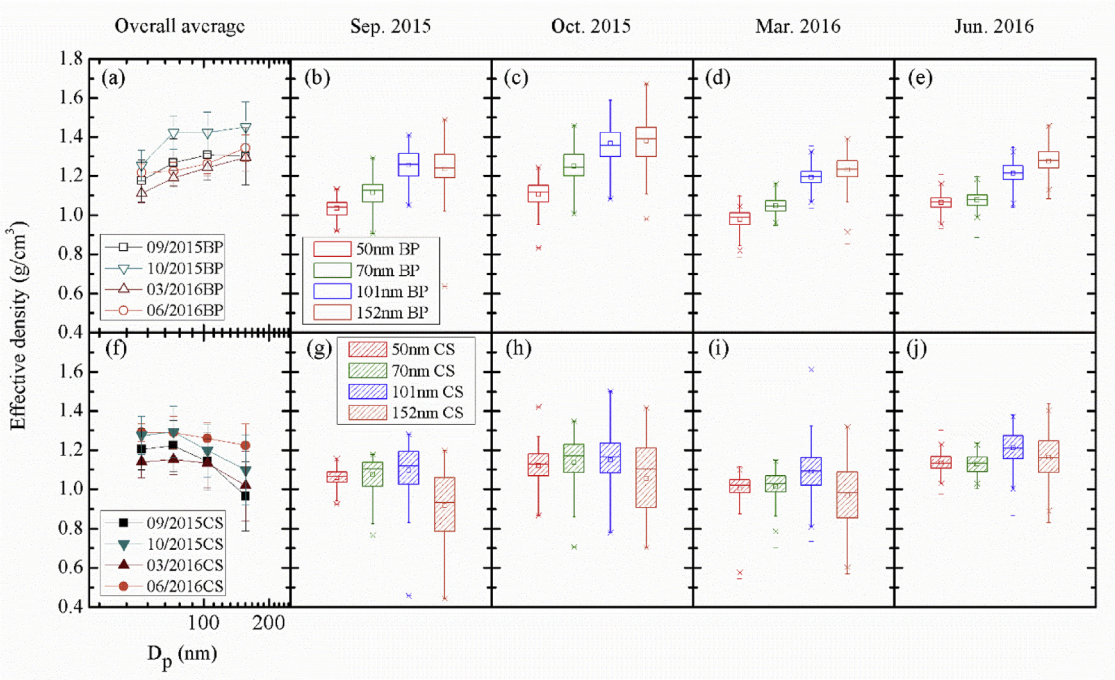

Fig. 6. Effective densities in different measurement periods for particles in BP and CS modes. The whiskers represent the 5th and 95th percentile, the two borders of box display the 25th and 75th percentile, and the band in each box denotes the median.

the measurements. Quiros et al. (2015) used the same approach for their measurements of vehicular exhaust particles to determine particle effective density. They used dioctyl sebacate (DOS) particles for their calibration tests. The difference between measured and bulk DOS spheres density remained below 9.4%. We expect similar uncertainties in our density determination. We conducted PSL calibrations before and after the measurement campaigns. The errors remained constant over the duration of the test program and no performance drift was observed.

3. Results and discussions

3.1. Overview of meteorological conditions

The meteorological conditions of all measurement periods are summarized in Table 1 and Fig. 3. The data were collected from the meteorology station at Riverside Municipal Airport, which is 9.6 km away from the sampling location. Riverside is dominated by desert-like climate. Solar radiation is strong throughout the year and as a result, the temperature and relative humidity (RH) vary dramatically during day and night time. Daily temperature reached its peak at around 3 p.m. and was the lowest at around 5 a.m. before sunrise. As expected, the opposite trend was observed for RH. The different ambient RH level could have affected water content of aerosols and aerosol effective density. During the measurement periods, Riverside was mostly dominated by eastward wind, from coastal areas of Los Angeles region. During Oct. 22–30, 2015, the nighttime was dominated by wind of moderate speed from North or Northeast. During other sampling periods, the westward wind appeared mostly in the early morning. Meteorological conditions during the sampling periods were comparable to the annual trends in the region.

3.2. Size-resolved effective density and fractal dimension

The size-resolved effective density values averaged over the whole measurement period for BP and CS modes are shown and compared with previous studies in Fig. 4. Error bars indicate standard deviations of the averaged values. During the BP mode measurements, particle effective density ranged from 1.17 to 1.28 g/cm^3 with slightly increasing trend as diameter increased in the 50–152 nm size range. This is similar to the previously reported average values, ranging from 1.29 to 1.40 g/cm^3, by Geller et al. (2006) who conducted ambient measurements in Riverside in 2005. Effective density measured by Levy et al. (2014) at Tijuana ranged from 1.21 to 1.31 g/cm^3 in the size range of our interest. Geller et al. (2006) showed decreasing density trends as the diameter increased. Average mAMS non-refractory measurements of composition in June 2016 period also indicated an increase in the fraction of inorganic species and a decrease in the hydrocarbon-like fraction of organic aerosol (HOA) with size in 50–152 nm range of density observations (Fig. 5). However, when we calculated time- and size-dependent material density of particles from chemical composition of mAMS measurements with the addition of a size-independent soot fraction, assuming particle sphericity and pure material densities of 1.75 g/cm^3 for ammonium nitrate and ammonium sulfate, 1.25 g/cm^3 for OA (to capture the higher contribution of fresh OA to the smaller sizes), and 1.8 g/cm^3 for BC, we did not observe a significant size-dependence (Cross et al., 2007; Middlebrook et al., 2012; Park et al., 2003). We speculate the discrepancy is in part due to the assumptions used in this calculation (e.g, size-independent soot fraction and particle sphericity), variability in the individual size distributions, as well as uncertainties of DMA-CPMA method. Further investigation is necessary to better understand size-dependent effective density.

Size resolved effective density averaged over the whole measurement period for the thermally treated (i.e. CS mode) ambient particles ranged from 1.22 g/cm^3 to 1.04 g/cm^3, and decreasing with diameter (Fig. 4). These are particles downstream of CS and therefore without significant semi-volatile components. The mAMS measurements during the CS mode showed negligible concentrations of non-refractory material, with average concentrations less than 6% of that in the BP mode, confirming that CS mode particles lack a significant contribution from semi-volatile components. It is expected that the majority of the non-volatile particles in our measurement range are soot particles. The average effective density profile resembled those of fresh soot measured in the lab by Maricq and Xu (2004) and Park et al. (2003) and they

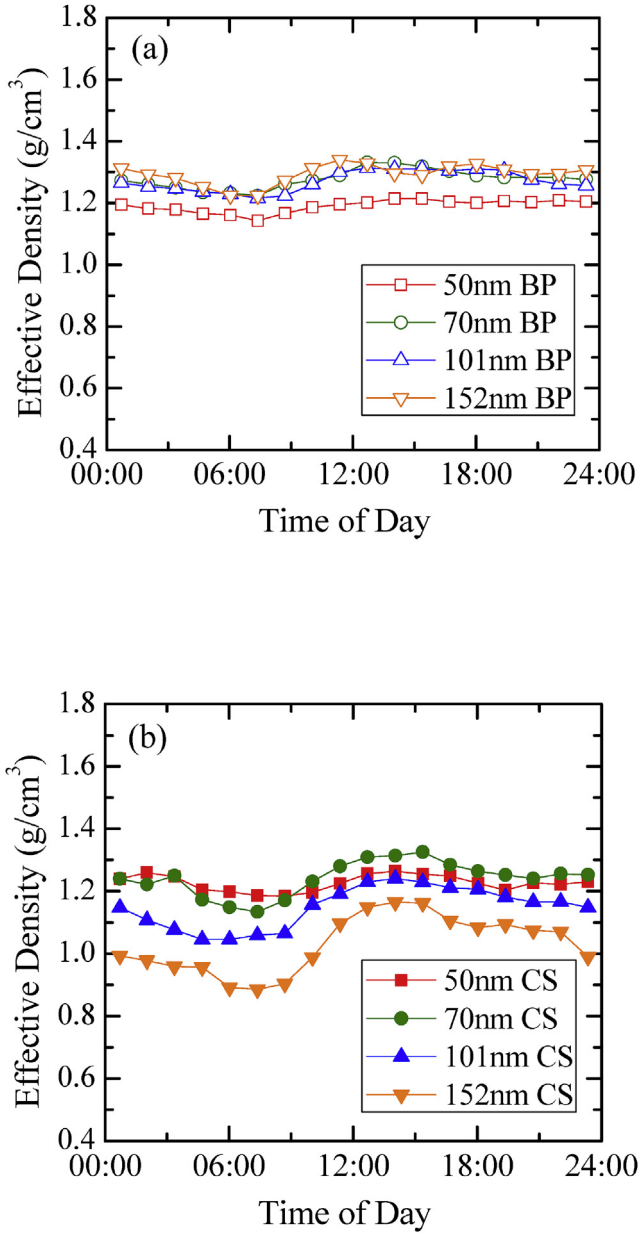

Fig. 7. Diurnal trends of the effective density averaged over the whole measurement period for BP (a) and CS (b) modes.

reported D_f = 2.3–2.4 for fresh diesel soot and D_f = 2.15 for flame generated fresh soot. However, the mass fractal dimension determined from this study was 2.85, indicating more compact shape. This value is very similar to D_f = 2.83 which Geller et al. (2006) reported for the measurements in Riverside.

Given the large variability in the averaged density values over the whole measurement period, we examine the trends of density with aerosol size in each sampling period separately (Fig. 6). Relatively large standard deviation for each period suggests effective density of ambient particles vary significantly daily and hourly. For ambient particles measured in BP mode, the measurement during October showed the highest and March the lowest effective density, while densities in September and June were comparable in terms of both average and median values. This may be the result of an interplay between transport and photochemistry. October period had lower temperatures than September. If photochemistry was the only driver, we expect to observe the highest densities during September. Densities for each measurement period are also plotted in box-whisker plots. Mean and median effective density of ambient particles in BP mode slightly increased as the particle size increased. Previous studies (Geller et al., 2006; Spencer et al., 2007) conducted in Riverside showed either nearly constant or decreasing densities as particle diameter increased while measurements in Shanghai China by Yin et al. (2015) showed an increase in effective density as particle size increased. The increasing trends of density with aerosol size will be further discussed in Section 3.3. Along with aerosol chemical composition results. Measurement conducted in March showed the least variability of the data while the one conducted in October showed the largest variability, consistent with wind direction variability in October (Fig. 3) and the potential for sampling different types/age aerosols. Effective densities of the non-volatiles particles (in CS mode) showed a different trend. Average density showed the smallest values for March and the largest values for June (Fig. 6). Additionally, mean and median effective density values were very similar for 50–101 nm particles while they decreased for the 152 nm particles during all measurement periods, except for the June period. The lowest variability in the CS-mode density of all particle sizes was also observed during June. We speculate that non-volatile particles may have been more compacted during the June period. Measurement during October period showed the largest variation of densities in CS mode, similar to what was observed in BP mode.

3.3. Diurnal trends of effective density

Diurnal trends of average effective density of the whole measurement period are shown in Fig. 7. Overall, density of particles in BP mode showed less variation during the day compared to those of CS mode. The 50 nm size particles showed the least variation in density for CS mode. This is likely due to a more compact initial morphology for small particles compared to larger size. For particles in CS mode, the largest size (i.e. 152 nm) showed the largest variation in density. Ghazi and Olfert (2013) reported smaller change in the effective density of organic coated soot for smaller initial particle size. Fig. 8 shows that particle effective density in BP mode varied from 0.88 g/cm^3 to 1.40 g/cm^3 while those in CS mode varied from 0.49 g/cm^3 to 1.26 g/cm^3.

For further investigation, diurnal profiles of particle effective density for each test measurement period were plotted in Fig. 8 as a function of selected mobility diameters. Strong diurnal trends were observed over all four sampling periods. The lowest values of effective density were observed during the morning rush hour while the values became larger after sunrise, when photochemistry becomes active, which is consistent with Levy et al. (2013)'s study in Houston. As mentioned above, we attribute the large variation in 2015 October period in part to the dynamic meteorological conditions, i.e. varying upstream wind speed and directions. The diurnal trends appeared more pronounced for particles in CS mode and larger sizes (101, 152 nm) compared to particles in BP mode and smaller particles (50 nm, 70 nm). We speculate that nonvolatile particles, which are most likely soot, may have undergone some degree of restructuring in CS mode measurements in the current study and that the degree of restructuring is likely related to the amount and type of volatile materials coated on the particles. Restructuring of soot aggregates is due to increased surface tension during evaporation of coated material; therefore, the extent of soot restructuring is material dependent (Bhandari et al., 2017). Evaporation of coated material can take place in the atmosphere when particles undergo dilution or temperature changes as well as during measurements in cases when a thermal denuder or catalytic stripper is used. Cross et al. (2010) reported the effect of coating and denuding on the soot optical properties using sulfuric acid and DOS as the coating material. Their study showed that there was a stronger restructuring of the soot core using sulfuric acid compared to DOS. Xue et al. (2009) also found restructuring of soot aggregates when they were first coated with glutaric acid and then denuded while there was no evidence for restructuring if coating was with succinic acid. Ghazi and Olfert (2013) also reported a dependence for soot restructuring on the mass of

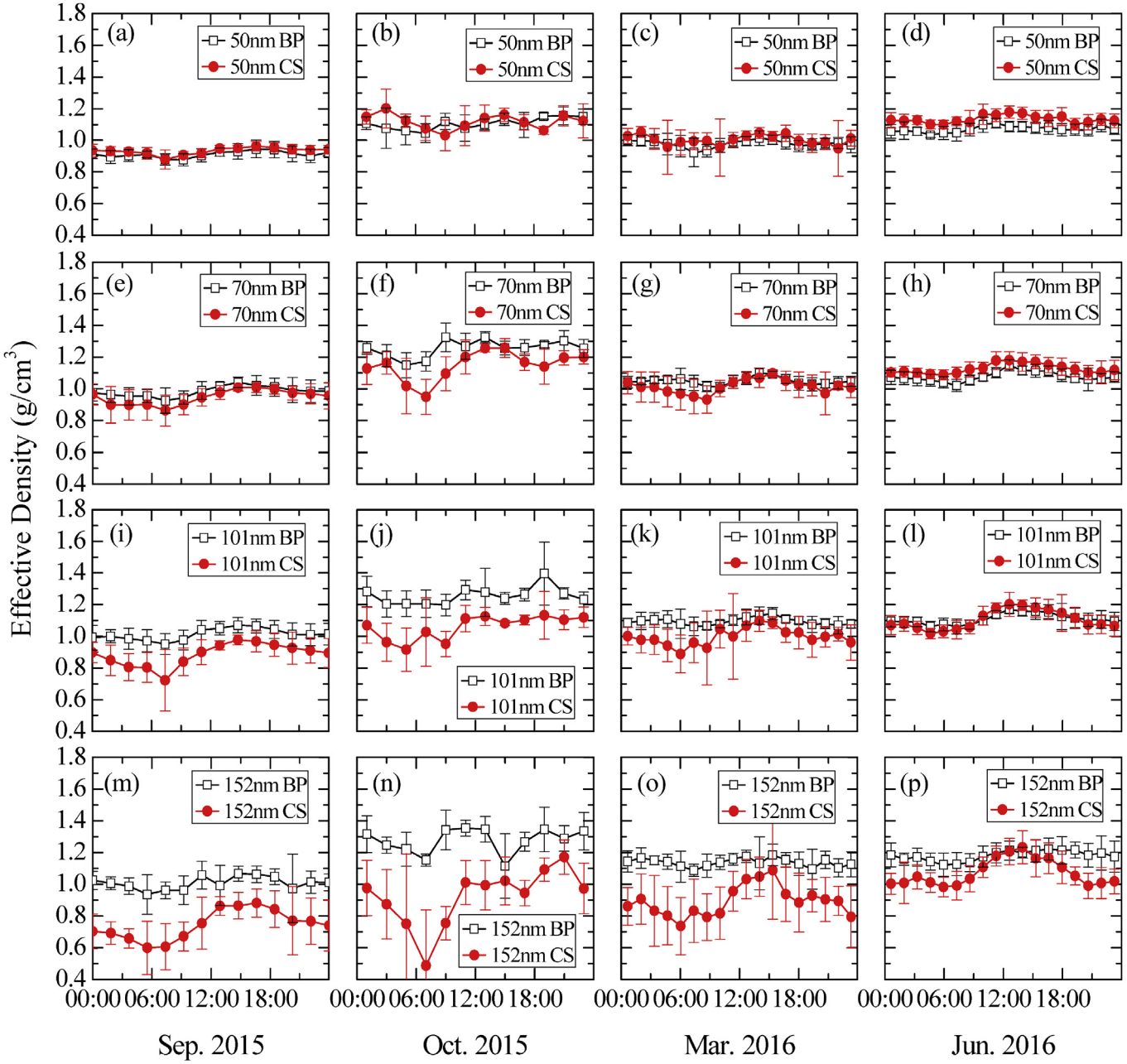

Fig. 8. Diurnal trends of the effective densities averaged over each measurement period for different selected sizes in BP (a) and CS (b) modes.

different coating material types until the amount of coating material exceeded a critical mass.

To further understand the influence of chemical composition on the particle effective density, mAMS data during 2016 June measurement period were analyzed for both BP and CS modes. Average, size-dependent mass fractions of the non-refractory species of BP mode are shown in Fig. 5. Ammonium sulfate (AS) and ammonium nitrate (AN) mass concentrations were calculated using the measured sulfate and nitrate mass concentrations while assuming full neutralization of these anions by ammonium. This assumption was supported by the bulk mass concentrations of ammonium, nitrate, and sulfate as measured by mAMS. Traces of oxygenated organic aerosol (OOA) and hydrocarbon-like OA (HOA) were estimated using simple parameterizations based on the mass distributions of ion fragments at *m/z* 44 and 57 amu (Ng et al., 2010). With this simple parameterization, the sum of OOA and HOA explained ~80% of total organics in the size range of density measurements. As apparent in Fig. 5, organics (more specifically, OOA) dominated the mass in the size range of the density measurement for BP mode while AN dominated the mass at larger sizes. Diurnal mass fractions of non-refractory species in sizes corresponding to the density measurements are shown in Fig. 9. AN mass fraction peaked ~2–10 a.m., consistent with favorable partitioning of ammonium nitrate, which is semivolatile, to the aerosol phase at lower temperatures and higher RH conditions during the early hours of the day (e.g., Drewnick et al., 2004; Jimenez et al., 2003). On the other hand, OA mass fraction showed a rapid increase ~9–11 a.m., with a gradual increase until 6pm, and a decrease afterwards. OA and AN mass fractions correlated positively and negatively with BP mode particle density averaged over the four size selections very well with r^2 0.78 and 0.62 respectively. However, particle effective density increased during the day when the fraction of lower density material (i.e. OA) increased and the fraction of the relatively denser AN decreased. An explanation for this counter-intuitive observation is that possibly the particles are internally mixed (as opposed to externally mixed) and OA filled the void areas of soot

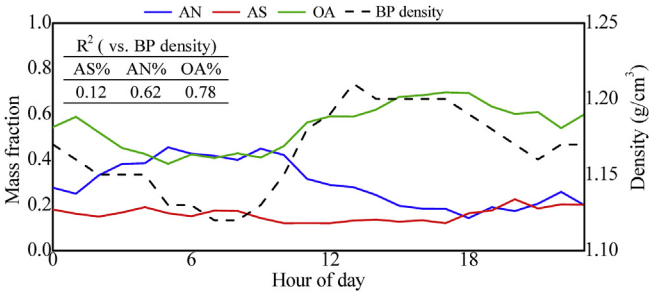

Fig. 9. The diurnal trends of mAMS non-refractory species and BP density averaged over the four measurement sizes, during June 2016 campaign. The mAMS species mass concentrations were summed over d_{va} = 70–268 nm corresponding to the density measurement size range. The hourly mass fractions were calculated based on the average of 50–80 data points during the campaign (corresponding to 1-min averages when all the mAMS integrated mass distributions resulted in positive mass concentrations). The density values for the four measured particle sizes were averaged by hour of the day.

aggregates in the size range of our interest better than AN. With the decrease in AN content, aerosol hygroscopicity and thus water content must have decreased too and so one could expect a higher aerosol density since OA is typically more dense than water. We found unimodal distributions in most of the size selected mass distribution measurements and a very weak bimodality was found only for a few measurements, indicating only one mixing state, likely internally mixed state, was prevalent in our size range of interest. The most common particle size distributions during all measurement periods are shown in Figure S1a. The particle size distributions in Figure S1b could be observed during a few early mornings in September 2015 and June 2016 measurement periods. Figure S2 shows mass distribution of the mobility size selected particles. We also compared PM mass, determined by the product of effective density and volumes from mobility diameter, with total –non-refractory aerosol mass determined by mAMS. Interestingly the PM mass determined by using particle size distributions and density profiles showed an excellent correlation with the measured OA (R^2 = 0.85) while the correlation became weaker with total mass by mAMS (R^2 = 0.72) in the size range from 50 to 152 nm in mobility diameter, supporting our hypothesis of OA filling the void of aggregates that provided the most surface area for adsorption of OA in the first place. Lack of a high correlation between PM mass determined by particle size distributions and inorganic mass is expected considering a large fraction of the inorganic species were present at sizes much larger than the size range of our particle size distribution measurement. Detailed comparisons among different metrics will be discussed in more detail in the follow up paper where the focus is to find a metric which best correlates with lung deposited PM mass. The mAMS measurement during CS mode resulted in negligible detection of non-refractory material, with average concentrations less than 6% of that in BP mode. We speculate the extent of restructuring of soot in the CS mode may have been related to the volatile mass fraction in the BP mode. Particles may have been restructured to some extent when volatile species coated on the soot surface evaporated in the CS. It should be noted that mobility size selection for density measurements was performed downstream of the CS indicating that the original particle sizes are larger than the selected sizes. This approach makes it difficult to understand the extent of atmospheric aging or restructuring of the soot before thermal denuding with the CS. Further studies with alternative sampling methods are necessary to untangle these effects.

4. Conclusions

Size-resolved effective density of 50–152 nm particles were measured by a (CS)-DMA-CPMA system, combined with parallel measurement of aerosol composition during 2015–2016 at Riverside, a well-known receptor site for pollution from LA area. The BP mode particle effective density ranged from 1.17 g/cm^3 to 1.28 g/cm^3, with a slightly increasing trend as particle size increased. On the other hand, effective density of particles in CS mode showed a decreasing density trend from 1.22 g/cm^3 to 1.04 g/cm^3, with a fractal dimension of 2.85. The effective density of BP and CS mode particles showed pronounced diurnal trends, with the lowest values observed during the morning traffic time and the peak in the early afternoon. The particle density of BP mode correlated well with OA mass. While diurnal density variation in BP mode seemed to be related with OA filling the void space of soot aggregate, diurnal density variation for CS mode particles appeared to be related to particle restructuring in the presence of semivolatile components. Although diurnal variations in the measured density were supported by time-dependent mAMS composition measurements, size-dependent density changes could not be clearly explained by the estimated material densities. Future studies should consider measuring mobility sizes before and after CS to quantify the amount and fraction of semivolatile components. The size-resolved density data will be used in a follow-up paper to estimate particle mass deposited in human lungs at the receptor site, Riverside CA for different seasons.

Acknowledgement

This study was funded by NSF grant # 1233038.

Appendix A. Supplementary data

Supplementary data related to this article can be found at http://dx.doi.org/10.1016/j.atmosenv.2018.05.063.

References

Abdul-Khalek, I.S., Kittelson, D.B., 1995. Real Time Measurement of Volatile and Solid Exhaust Particles Using a Catalytic Stripper (SAE Technical Paper). .
Bhandari, J., China, S., Onasch, T., Wolff, L., Lambe, A., Davidovits, P., Cross, E., Ahern, A., Olfert, J., Dubey, M., 2017. Effect of thermodenuding on the structure of nascent flame soot aggregates. Atmosphere 8, 166.
Cross, E.S., Onasch, T.B., Ahern, A., Wrobel, W., Slowik, J.G., Olfert, J., Lack, D.A., Massoli, P., Cappa, C.D., Schwarz, J.P., 2010. Soot particle studies—instrument inter-comparison—project overview. Aerosol. Sci. Technol. 44, 592–611.
Cross, E.S., Slowik, J.G., Davidovits, P., Allan, J.D., Worsnop, D.R., Jayne, J.T., Lewis, D.K., Canagaratna, M., Onasch, T.B., 2007. Laboratory and ambient particle density determinations using light scattering in conjunction with aerosol mass spectrometry. Aerosol. Sci. Technol. 41, 343–359.
DeCarlo, P.F., Slowik, J.G., Worsnop, D.R., Davidovits, P., Jimenez, J.L., 2004. Particle morphology and density characterization by combined mobility and aerodynamic measurements. Part 1: Theory. Aerosol Sci. Technol 38, 1185–1205 doi: 1110.1080/027868290903907.
Drewnick, F., Schwab, J.J., Jayne, J.T., Canagaratna, M., Worsnop, D.R., Demerjian, K.L., 2004. Measurements of ambient aerosol composition during PMTACS-NY 2001 using an aerosol mass spectrometer. Part I: mass Concentrations. Aerosol. Sci. Technol. 38, 92–103 doi: 110.1080/02786820390229507.
Geller, M., Biswas, S., Sioutas, C., 2006. Determination of particle effective density in urban environments with a differential mobility analyzer and aerosol particle mass analyzer. Aerosol Sci. Technol. 40, 709–723.
Ghazi, R., Olfert, J., 2013. Coating mass dependence of soot aggregate restructuring due to coatings of oleic acid and dioctyl sebacate. Aerosol. Sci. Technol. 47, 192–200.
Jimenez, J.L., Jayne, J.T., Shi, Q., Kolb, C.E., Worsnop, D.R., Yourshaw, I., Seinfeld, J.H., Flagan, R.C., Zhang, X., Smith, K.A., Morris, J., Davidovits, P., 2003. Ambient aerosol sampling with an aerosol mass spectrometer. J. Geophys. Res. 108, 8425, doi: 8410.1029/2001JD001213.
Kinney, P.D., Pui, D.Y., Mulliolland, G.W., Bryner, N.P., 1991. Use of the electrostatic classification method to size 0.1 μm SRM particles—a feasibility study. Journal of Research of the National Institute of Standards and Technology 96, 147.
Levy, M.E., Zhang, R., Khalizov, A.F., Zheng, J., Collins, D.R., Glen, C.R., Wang, Y., Yu, X.Y., Luke, W., Jayne, J.T., 2013. Measurements of submicron aerosols in Houston, Texas during the 2009 SHARP field campaign. J. Geophys. Res.: Atmosphere 118.
Levy, M.E., Zhang, R., Zheng, J., Tan, H., Wang, Y., Molina, L.T., Takahama, S., Russell, L., Li, G., 2014. Measurements of submicron aerosols at the California–Mexico border during the Cal–Mex 2010 field campaign. Atmos. Environ. 88, 308–319.
Maricq, M.M., Xu, N., 2004. The effective density and fractal dimension of soot particles from premixed flames and motor vehicle exhaust. J. Aerosol Sci. 35, 1251–1274.
Martin, S., 2003. Nano Particle Formation in the Exhaust of Internal Combustion Engines.
McMurry, P.H., Wang, X., Park, K., Ehara, K., 2002. The relationship between mass and mobility for atmospheric particles: a new technique for measuring particle density. Aerosol Sci. Technol. 36, 227–238.

Middlebrook, A.M., Bahreini, R., Jimenez, J.L., Canagaratna, M.R., 2012. Evaluation of composition-dependent collection efficiencies for the aerodyne aerosol mass spectrometer using field data. Aerosol. Sci. Technol. 46, 258–271.
Mulholland, G.W., Bryner, N.P., Croarkin, C., 1999. Measurement of the 100 nm NIST SRM 1963 by differential mobility analysis. Aerosol. Sci. Technol. 31, 39–55.
Ng, N., Canagaratna, M., Jimenez, J., Zhang, Q., Ulbrich, I., Worsnop, D., 2010. Real-time methods for estimating organic component mass concentrations from aerosol mass spectrometer data. Environ. Sci. Technol. 45, 910–916.
Oberdörster, G., Oberdörster, E., Oberdörster, J., 2005. Nanotoxicology: an emerging discipline evolving from studies of ultrafine particles. Environ. Health Perspect. 113, 823.
Olfert, J., Collings, N., 2005. New method for particle mass classification—the Couette centrifugal particle mass analyzer. J. Aerosol Sci. 36, 1338–1352.
Olfert, J., Symonds, J., Collings, N., 2007. The effective density and fractal dimension of particles emitted from a light-duty diesel vehicle with a diesel oxidation catalyst. J. Aerosol Sci. 38, 69–82.
Park, K., Cao, F., Kittelson, D.B., McMurry, P.H., 2003. Relationship between particle mass and mobility for diesel exhaust particles. Environ. Sci. Technol. 37, 577–583.
Petzold, A., Kramer, H., Schönlinner, M., 2002. Continuous measurement of atmospheric black carbon using a multi-angle absorption photometer. Environ. Sci. Pollut. Res. 78–82.
Quiros, D.C., Hu, S., Hu, S., Lee, E.S., Sardar, S., Wang, X., Olfert, J.S., Jung, H.S., Zhu, Y., Huai, T., 2015. Particle effective density and mass during steady-state operation of GDI, PFI, and diesel passenger cars. J. Aerosol Sci. 83, 39–54.
Rissler, J., Nordin, E.Z., Eriksson, A.C., Nilsson, P.T., Frosch, M., Sporre, M.K., Wierzbicka, A., Svenningsson, B., Löndahl, J., Messing, M.E., 2014. Effective density and mixing state of aerosol particles in a near-traffic urban environment. Environ. Sci. Technol. 48, 6300–6308.
Spencer, M.T., Shields, L.G., Prather, K.A., 2007. Simultaneous measurement of the effective density and chemical composition of ambient aerosol particles. Environ. Sci. Technol. 41, 1303–1309.
Symonds, J.P., Reavell, K.S.J., Olfert, J.S., 2013. The CPMA-electrometer system—a suspended particle mass concentration standard. Aerosol. Sci. Technol. 47, i–iv.
Turpin, B.J., Lim, H.-J., 2001. Species contributions to PM2. 5 mass concentrations: revisiting common assumptions for estimating organic mass. Aerosol Sci. Technol. 35, 602–610.
Xue, H., Khalizov, A.F., Wang, L., Zheng, J., Zhang, R., 2009. Effects of coating of dicarboxylic acids on the mass− mobility relationship of soot particles. Environ. Sci. Technol. 43, 2787–2792.
Yin, Z., Ye, X., Jiang, S., Tao, Y., Shi, Y., Yang, X., Chen, J., 2015. Size-resolved effective density of urban aerosols in Shanghai. Atmos. Environ. 100, 133–140.